Simulating recrystallization through cellular automata and genetic algorithms

R Dewri[1] **and N Chakraborti**[2,3]

[1] Department of Mathematics and Computing, Indian Institute of Technology, Kharagpur 721 302, India
[2] Department of Metallurgical and Materials Engineering, Indian Institute of Technology, Kharagpur 721 302, India

E-mail: nchakrab@iitkgp.ac.in

Abstract

A simulation of the recrystallization process was conducted by coupling a cellular automation with a lookup table that evolved using genetic algorithms. Through an evolutionary inverse modelling, the rate of recrystallization, and the grain size distribution were successfully optimized and the recrystallized microstructure was acceptably predicted.

1. Introduction

Any piece of metal, when mechanically or otherwise deformed, is raised to a state of higher free energy. Typically, a further addition of thermal energy through the annealing process carried out at a temperature above half of its melting point, removes many of the defects in the crystal lattice. Following this *recovery* stage, a new set of grains first nucleate and then start to grow, constituting the *recrystallization* process, resulting in a newer microstructure and a lower free energy [1].

Simulation of the recrystallization microstructure has been described in a number of studies [2–7]. The major strategies employed by various researchers are cellular automata (CA), a combination of CA and Monte Carlo technique, CA aided by a finite element analysis and also a popular version of simulated annealing—the metropolis algorithm.

Without any exceptions, some complex analytical model was, however, utilized in all the recrystallization studies cited above. This rendered the computing scheme fairly cumbersome. In addition, the presence of several model parameters for which precise values were lacking often rendered the final predictions open to a reasonable doubt. What we have presented here is an alternate strategy devoid of any analytical models. Only a few commonsensical rules have

[3] Author to whom any correspondence should be addressed.

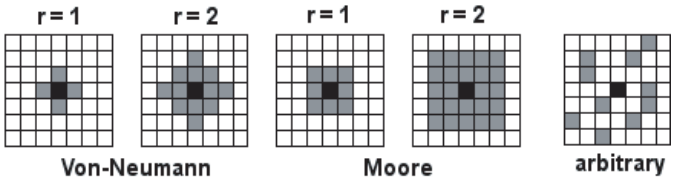

Figure 1. Schematics of possible neighbourhoods for the cell shown in dark black. The lighter black cells are in its neighbourhood. The maximum cell radius is denoted as r.

been used here; available experimental data have been utilized through an inverse procedure, leading to a simple, phenomenological description of the process, and it takes the fullest advantage of an emerging evolutionary computing scheme [8]. This work thus constitutes an optimized simulation method of the *recrystallization* phenomenon through a judicious coupling of two widely discussed evolutionary algorithms, CA [8–10] and the genetic algorithm (GA) in its binary form [10, 11]. This has been further augmented through the introduction of a lookup table, a newer approach that has so far not been tried out for a problem of this category. The principles involved are elaborated in the following sections.

2. The background

A physical event could be successfully simulated through CA assuming both time and space to be discrete. Here, the physical space can be looked upon as a concatenation of some discrete *cells*, each in one of the admissible *states* defined *a priori*. At any discrete time step, the state of a cell will be determined by its state in the previous time step, the set of rules prescribed for its transition, as well as the state of the other cells in its *neighbourhood*, which can be defined in more than one way, as elaborated in figure 1.

In an earlier work [12] we had attempted to simulate the recrystallization process by coupling a CA with differential evolution (DE), a real coded variant of GAs, known to be a robust optimizer [11–13]. Two possible states were assigned to the cells. The binary variable 1 denoted a recrystallized state, and 0 implied that the cell was unrecrystallized. A Moore neighbourhood with $r = 2$ was assumed, and a few simple phenomenological transformation rules were implemented. In any metallic specimen the regions that are relatively heavily deformed are more prone to nucleation. The entire physical space is thus divided into periodically placed regions of high and low rates as shown schematically in figure 2. Among the variables considered were (i) nucleation rate in the CA array (n_r)[4], (ii) transition probability for nucleation (P_t), (iii) square size or the periodicity of the spatial distribution of the high probability band (S), (iv) area fraction of the high probability band within each square (α), and (v) ratio of transition probability in the high probability band to that in the low probability zone (ρ_{ratio}).

An inverse modelling approach was followed to determine these crucial parameters using the experimental recrystallization data (i.e. fraction recrystallized as a function of time) for the single crystal of iron already in hand [14], and differential evolution was used to optimize values of the five crucial parameters mentioned above, as shown schematically in figure 3. Although the rate of nucleation and the fraction transformed could be acceptably predicted

[4] In many traditional models n_r is taken as an input parameter. The critical nuclei sizes are, however, very small, defying accurate experimental determination of the nucleation rate and its mesoscopic distribution, which, in turn, brings in significant inaccuracies in the prediction. This problem has been circumvented here through the inverse approach by treating n_r as a variable, and arriving at its optimized value along with the other parameters.

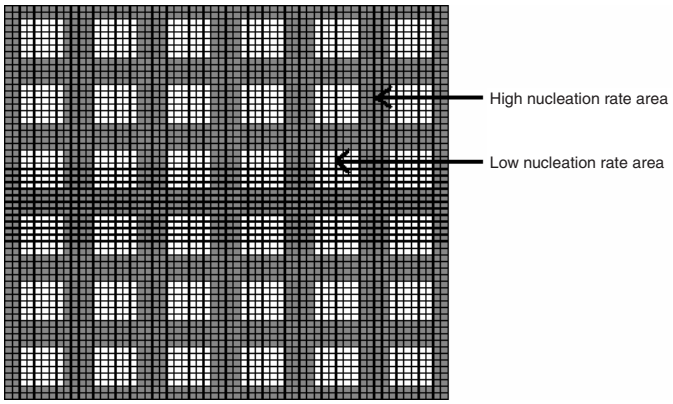

Figure 2. The regions of high and low nucleation.

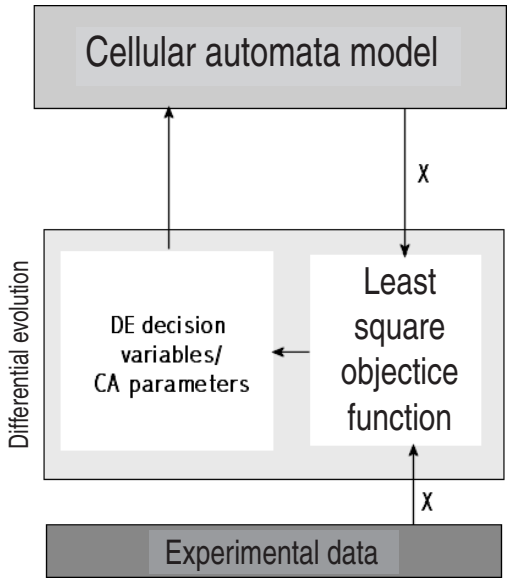

Figure 3. Computational scheme used in [12].

through this model, it had no provisions to compute the orientations of the different grains during their growth, and consequently, could not simulate the grain size distribution, and for that matter, the microstructure of the recrystallized grains.

During this work we have further augmented this model to overcome these shortcomings. The pertinent details are provided below.

3. A modified scheme

As a first attempt to simulate the differential grain orientation, we have employed a multiple lattice state system where a particular state is mapped onto a unique grain orientation. The rules of the automata are kept the same; however, transition rules from one grain state to the next has been added to it. These transitions are decided by the following: (i) an untransformed cell

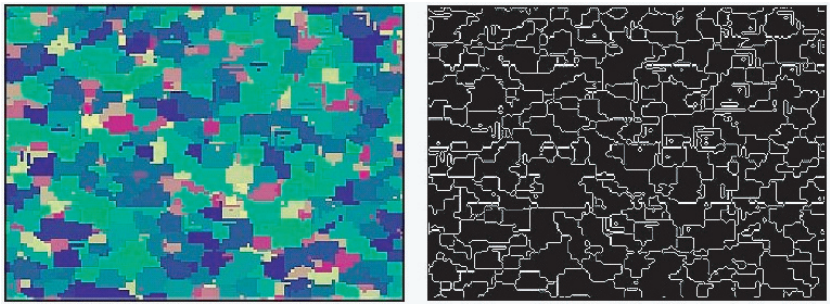

Figure 4. Simulated microstructure and the grain boundaries obtained using the edge detection algorithm.

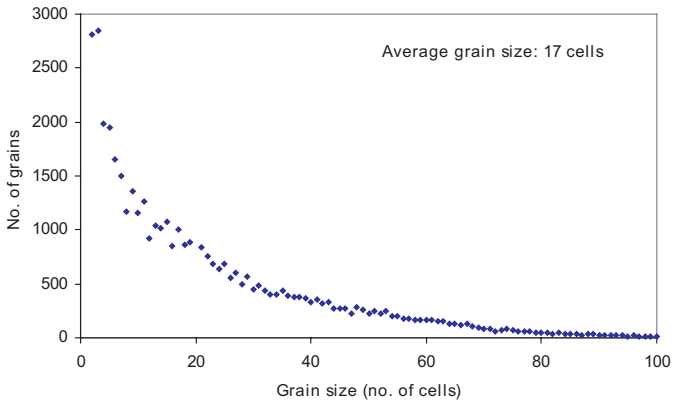

Figure 5. The frequency distribution of the grain size.

takes the orientation of one of its neighbours with a given probability, (ii) an untransformed cell being nucleated assumes a new state. It has to be noted that once a cell has been assigned a state with a preferred orientation, it will not change for the entire run of the simulation, meaning that the model does not take into account the idea of grains growing over one another. Once the whole lattice becomes recrystallized, the simulation virtually stops. Moreover, nucleation and the growth processes are simultaneous and new nuclei appear at every step of the transformation, hence the expected distribution of the grain sizes is exponential. Figure 4 shows the simulated microstructure over a 1000×1000 lattice[5], using this modified scheme. An edge detection algorithm has been applied on this microstructure to see the exact network of cells appearing in it. The frequency distribution of the grain size is plotted in figure 5.

In order to check for theoretical consistency of the observed grain size distribution, we obtained a probability distribution of the reduced grain area $\acute{A}$, taken as the ratio of the overall area A covered by a grain of a particular size to the mean grain area. For continuous nucleation, a simple expression for this probability has been proposed as [15].

$$P(\acute{A}) = \exp(-\acute{A}). \tag{1}$$

Figure 6 shows the theoretical and observed probability distributions in this regard. The distribution deviates noticeably from the theoretical one for grains of small sizes, once again

[5] An area of 0.25 cm^2 is represented by a total of 10^6 cells in the lattice.

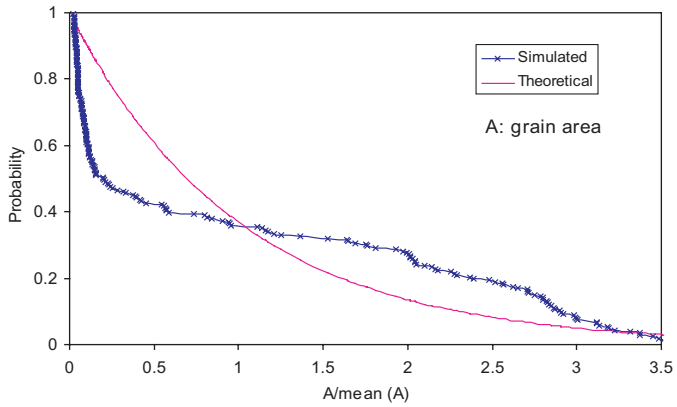

Figure 6. Histograms of grain size distribution.

attributable to the assumed nucleation probability distribution and its effects. A Kolmogorov–Smirnov goodness-of-fit test [16] also shows that the test statistic value (the maximum absolute deviation between the two data sets) is way above the critical value (generally equal to $c/\sqrt{n}$, c being a constant dependent on the distribution, and n the number of data points). Thus, further changes in the computing procedure appear to be in order. We have now introduced a lookup table coupled with a binary GA to augment the simulation. Further details follow.

4. Computing with binary GA and a lookup table

The approach adopted henceforth is to determine the transition rules in the form of a lookup table that comes up with an acceptable grain size distribution while minimally deviating from the already obtained good fits of the recrystallization fraction to the experimental data. A lookup table for a CA model is a set of transition rules specifying the outcome of every possible configuration of its neighbours. Unlike the previous approach, the high–low recrystallization probability areas have been discarded here in order to avoid the accumulation of relatively larger grain sizes at the high probability zones. It needs to be pointed out at this stage that the periodicity of the high and low nucleation regimes depicted in figure 2 is rather idealistic. The exact frequency of their occurrence is actually quite difficult to ascertain; even if they appear in some realistic situations, their presence would, however, result in the formation of high angle boundaries. For single crystals, polygonization remains the major process, and no such boundaries are likely to form, unless the total duration considered is very large. The periodicity shown in figure 2, therefore, can be safely neglected for the single crystals of iron for which the present simulation would be valid. Thus, henceforth, our CA model just becomes a two-dimensional array of 1000×1000 cells, where the changes in the states are being decided by the lookup table, which in turn, evolves through a GA. Also, for the sake of reducing the computational complexity, the 25-cell Moore neighbourhood has been replaced by a 12-cell Von Neumann neighbourhood. This simply resulted in a faster search and a speedy execution of the code with no apparent loss of accuracy. Grain orientation is embedded in the model as in the earlier cases.

Although the lookup table is the only component influencing our simulations, unlike a simple functional optimization problem, the overall simulation results are, however, not just direct consequences of this variable in the optimization process. A lookup table in this case is actually a collection of blocks of information (and not variable values) to be used by the

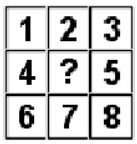

Figure 7. Numbering scheme of the Von Neumann neighbourhood.

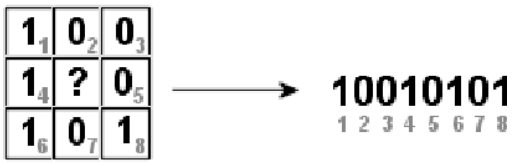

Figure 8. Arrangement of the states in a Von Neumann neighbourhood.

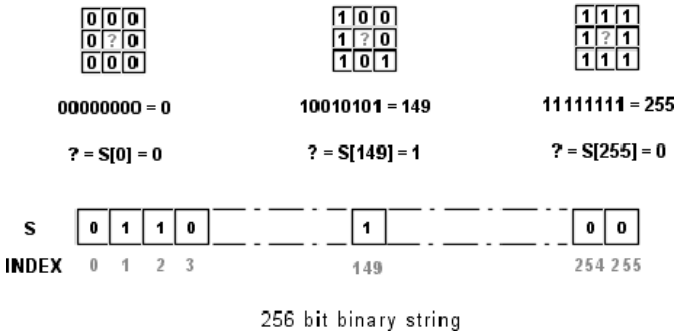

Figure 9. Obtaining the new state from the lookup table.

automata as a set of guidelines for evolving through multiple cycles. The encoding scheme for this algorithm requires further elaboration, as provided below.

5. The new solution strategy

An 8-cell neighbourhood, with two states in each cell, has got $2^8 = 256$ possible configurations of states. As indicated before, the two states here are 1 (recrystallized) or 0 (unrecrystallized). A 256 bit binary string will thus be used to represent each of the possible configurations. In the environment of GAs, a population of such strings will be considered, and it will evolve through the traditional evolutionary processes like selection, crossover, and mutation [10, 11]. A numbering scheme is employed to determine which configuration corresponds to which bit of the string. The eight neighbouring cells are numbered in a linear order starting from the top left corner, as shown in figure 7. The states of each of the neighbouring cells are arranged in an order specific to this numbering scheme. Figure 8 clarifies this.

The decoded value of the binary bit pattern 10010101 in our example is 149. To determine the index, the central cell, shown with a query mark in figure 8, the 149th bit of a 256 bit *individual* is picked up from the lookup table. Its bit value determines the new state of the centre cell to be obtained. The process is further illustrated in figure 9 for three typical central cells, including the one that has just been mentioned. Note that we are assuming a zero index starting.

The entire lookup table is thus encoded into a 256 bit binary string. A simple binary GA can then be applied to a randomly generated population of such strings. The mean square

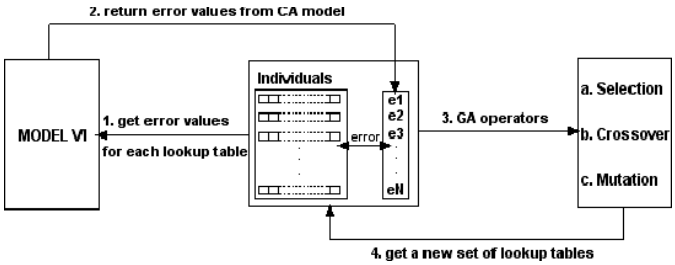

Figure 10. Schematics of control flow in one generation of the binary GA.

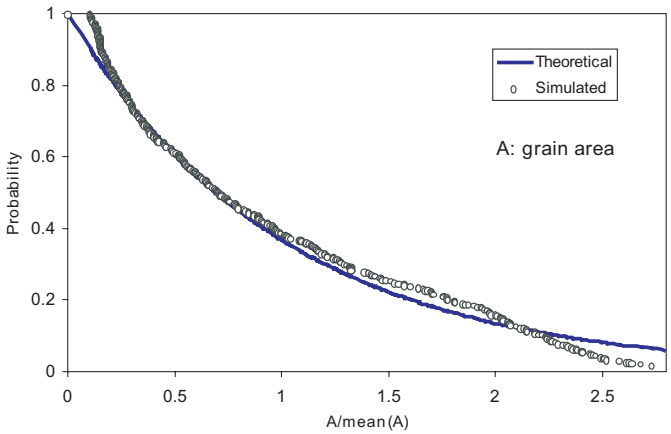

Figure 11. Grain size distributions obtained using the lookup table and binary GA with a nucleation rate of $500\,s^{-1}$.

error for the grain size distribution with respect to the theoretical one is calculated from the model, using each of these tables, and is subjected to minimization. During a simulation run, the lookup table is consulted only if a cell is in an unrecrystallized state (state 0); otherwise the computation passes on to the next cell. Crossover and mutation probabilities are fixed at 0.8 and 0.01, respectively. Thus, a population size of 30 has evolved for 50 generations to provide an acceptable microstructure. Figure 10 shows the flow of control during the execution of one generation of the binary GA.

6. Results and discussion

The results from the above optimization are as follows. Figure 11 indicates a good match between the theoretical and simulated data for iron single crystals [14]. Grains nearing the average size are almost in conformation to the theoretically expected value. The model slightly deviates from the expected values for too small or too large grains. The deviations are explained by considering that the number of grids is not large enough to correctly estimate grains of very small sizes, while for grains of relatively larger sizes the growth dynamics after recrystallization has not been simulated in this study.

However, the accuracy of the recrystallized area fraction predicted by the model in this case has come at a price. The predicted recyrstallization curve still substantially deviates from the experimental data, as can be seen in figure 12. The nucleation rate, which was fixed at $500\,s^{-1}$,

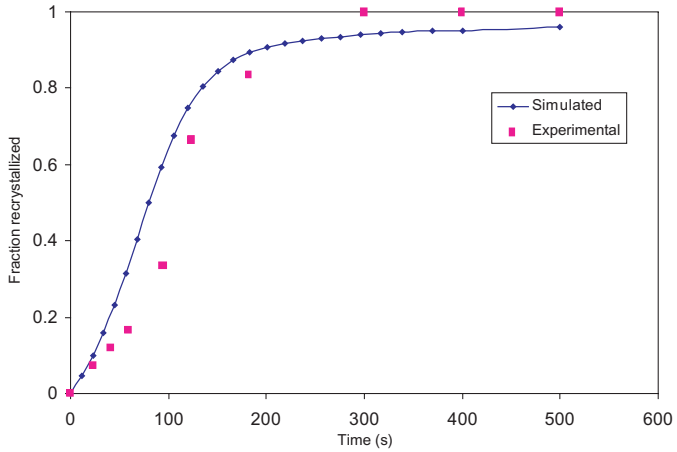

Figure 12. Plot showing area fraction recrystallized over time (modelled using a recrystallization rate of $500\,s^{-1}$).

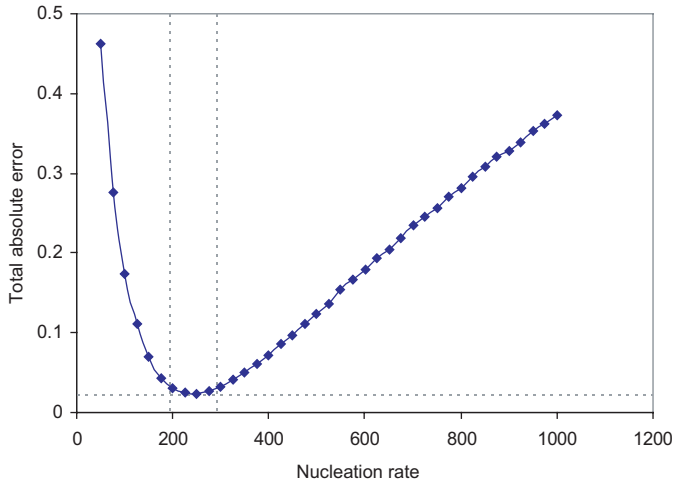

Figure 13. Effect of nucleation rate on total absolute error of recrystallized fraction.

plays an important role in deciding the kinetics of this process. A very large nucleation rate effectively pushes the recrystallization process in the beginning, causing a major deviation of the predicted values from the experimental data.

Figure 13 shows the variation in the total absolute error in the predicted area fraction recrystallized with respect to the experimental data. The errors are calculated with the lookup table generated by the aforementioned optimization process. As can be seen, the errors are high for relatively high or low nucleation rates. For low nucleation rates, the model cannot accommodate the steep rise in the fraction recrystallized during the intermediate period (i.e. the time between 60 and 200 s), while for a too high nucleation rate the number of recrystallized grains grows tremendously in less than 60 s, and as expected, it becomes equally difficult to capture this effect through this model.

The modified optimization process, however, gives a better prediction of the area fraction recrystallized. Figure 14 captures the predicted values in comparison to the experimental ones.

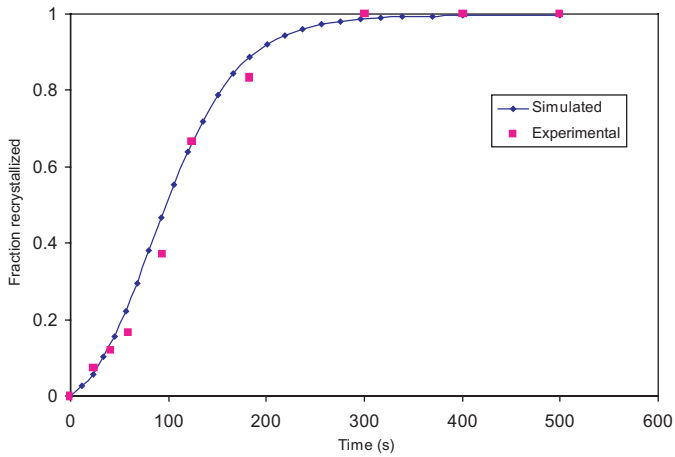

Figure 14. Plot showing area fraction recrystallized over time (modelled using a nucleation rate of 200 s^{-1}).

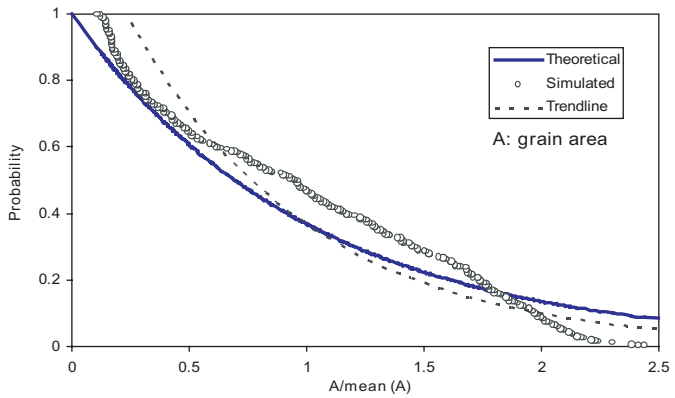

Figure 15. Grain size distribution obtained using a nucleation rate of 200 s^{-1}.

The fit obtained is much better in this case as compared to the previous one. However, ironically, the grain size distribution suffers and fails to maintain the previously obtained accuracy (figure 15). The trend line shows the exponential curve that best fits the data points from the simulation. It should be noted that the prediction in both cases has been considerably better than that with the earlier model.

Given the nature of the results obtained, the lookup tables obtained during the optimization processes are analysed. Figure 16 shows a symbolic representation of the lookup tables obtained in the form of a 16×16 array. The 256 bit binary string can be obtained by traversing the array row wise, starting at the top left corner. All white cells are to be interpreted as a 0, otherwise 1. As such, analysing the lookup tables in this format is not feasible; hence we determine the probability with which a cell gets recrystallized, given that it has got n already recrystallized neighbours. It can be seen from figure 17 that these probabilities are higher (or almost equal) for all configurations in the second lookup table. This has an effect in deciding the total fraction recrystallized over the entire simulation run (95.2% in the first case and 99.5% in the second case), which should be fully completed according to the experimental data.

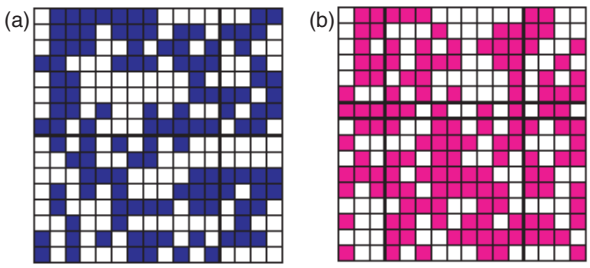

Figure 16. Symbolic representation of the 256 bit lookup tables obtained with nucleation rates of (*a*) $500\,s^{-1}$ and (*b*) $200\,s^{-1}$. To be read row wise starting from top left corner; white as 0 and dark as 1.

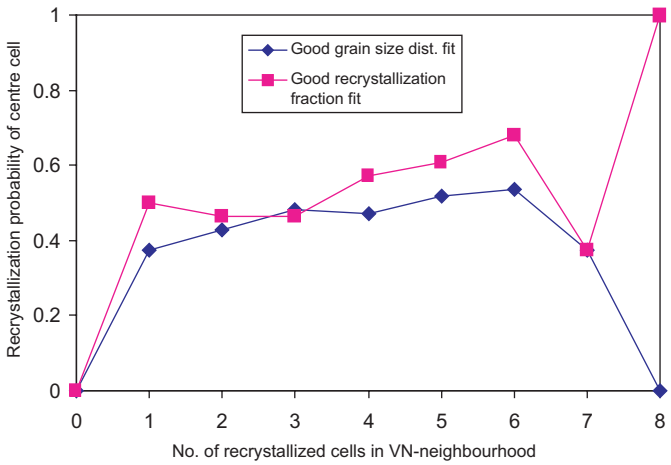

Figure 17. Recrystallization probability of centre cell with an 8-cell neighbourhood.

The overall recrystallized fraction shows a sigmoidal pattern of growth, where a steady increase during the initial 60 s is followed by an almost linear regime, which finally starts saturating fast. The probability data provided in figure 17 also follow a similar trend. What differentiates the two tables is the probability value when all the neighbouring cells are recrystallized. In the first case, the probability starts dropping towards the end, finally coming down to zero. Although this accommodates the saturating trend of the experimental data towards the end, the recrystallization process following this probability would never be complete, as an unrecrystallized cell surrounded by other predominantly recrystallized neighbours would never be able to transform. The second lookup table took care of this by first considerably dropping the probability and then again increasing it at the end.

The growth of the grains in the second case has been faster than expected, with a majority of the points near the average grain size having probabilities higher than the theoretical one. High recrystallization probabilities during the runs have accounted for this behaviour. The first case shows a better linearity for the intermediate probabilities (1 through 6) and hence might be a reason for the steady growth that has been observed. Also, complete grain growth statistics cannot be obtained from the current model, since post recrystallization dynamics have not been incorporated and, therefore, deviations between the theoretical predictions and model observations are likely. However, by specifying different nucleation rates, a trade-off between the grain size distribution and the area fraction recrystallized can be obtained.

A multi-objective formulation might help in determining it and future research needs to be directed towards that.

7. Concluding remarks

The simplicity gained by adopting the present methodology is tremendous in the sense that it does not require a very rigorous mathematical description of the physical process. The fact that no *a priori* estimation of sensitive and crucial parameters, like the rate of nucleation, is required, where the available experimental data are often known to vary by orders of magnitude, also becomes highly advantageous in a real situation. Like most of its predecessors the present approach is yet to be fully effectively used in every regime of the recrystallization process. However, the data set used in this study [14] was also analysed in a previous work using various approaches [17]. Our model already produced a comparable, if not better, simulation of the same experimental results. Nonetheless, the model could perhaps be further augmented, and it can very easily constitute a next phase of this study. It would also be interesting to see if the inverse modelling can be made better by adopting a different lattice geometry, specifically a triangular one. A square lattice is not capable of capturing the grain geometry as well as a triangular one. The rules, then, will also have to be correspondingly changed.

In recent times hot rolling and other deformation processes have been effectively simulated using evolutionary approaches [11, 18, 19]. The capability of simulating the post-rolling, heat treated microstructures can now be coupled with it, following the strategy adopted in this study, which could be of immense importance to the iron and steel industry, in particular.

Acknowledgment

Helpful discussions with Professor I Manna are very much appreciated.

References

[1] Haasen P 1996 *Physical Metallurgy* (Cambridge: Cambridge University Press)
[2] Ding R and Guo Z X 2004 *Mater. Sci. Eng.* A **365** 172
[3] Kugler G and Turk R 2004 *Acta Mater.* **52** 4659
[4] Gottstein G and Sebald R 2001 *J. Mater. Process. Technol.* **117** 282
[5] Sarma G B and Radhakrishnan B 2004 *Mater. Sci. Eng.* A **385** 91
[6] Radhakrishnan B, Sarma G B and Zacharia T 1998 *Scr. Mater.* **39** 1639
[7] Tewari A and Gokhale A M 2004 *Mater. Sci. Eng.* A **385** 332
[8] Wolfram S 1986 *Theory and Applications of Cellular Automata (Advanced Series on Complex Systems* vol 1*)* (Singapore: World Scientific)
[9] Wolfram S 2002 *New Kind of Science* (USA: Wolfram Media)
[10] Mitchell M 1998 *An Introduction to Genetic Algorithms* (New Delhi: Prentice-Hall)
[11] Chakraborti N 2004 *Int. Mater. Rev.* **49** 246
[12] Rane T D, Dewri R, Ghosh S, Mitra K and Chakraborti N 2004 *Modeling the Recrystallization Process Using Inverse Cellular Automata and Genetic Algorithms: Studies Using Differential Evolution* unpublished research
[13] Price K and Storn R 1997 Differential evolution *Dr. Dobb's J.* **22** 18
[14] Vandermeer R A and Rath B B 1989 *Metall. Trans.* A **20** 391
[15] Mulheran A 1994 *Acta Metall. Mater.* **42** 3589
[16] Massey F J 1951 *J. Am. Stat. Assoc.* **46** 68
[17] Davies C H J 1997 *Scr. Mater.* **36** 35
[18] Chakraborti N and Kumar A 2003 *Mater. Manuf. Processes* **18** 433
[19] Nandan R, Rai R, Jayakanth R, Moitra S, Mukhopadhyay A and Chakraborti N 2005 *Mater. Manuf. Processes* at press